

Supplementary Materials

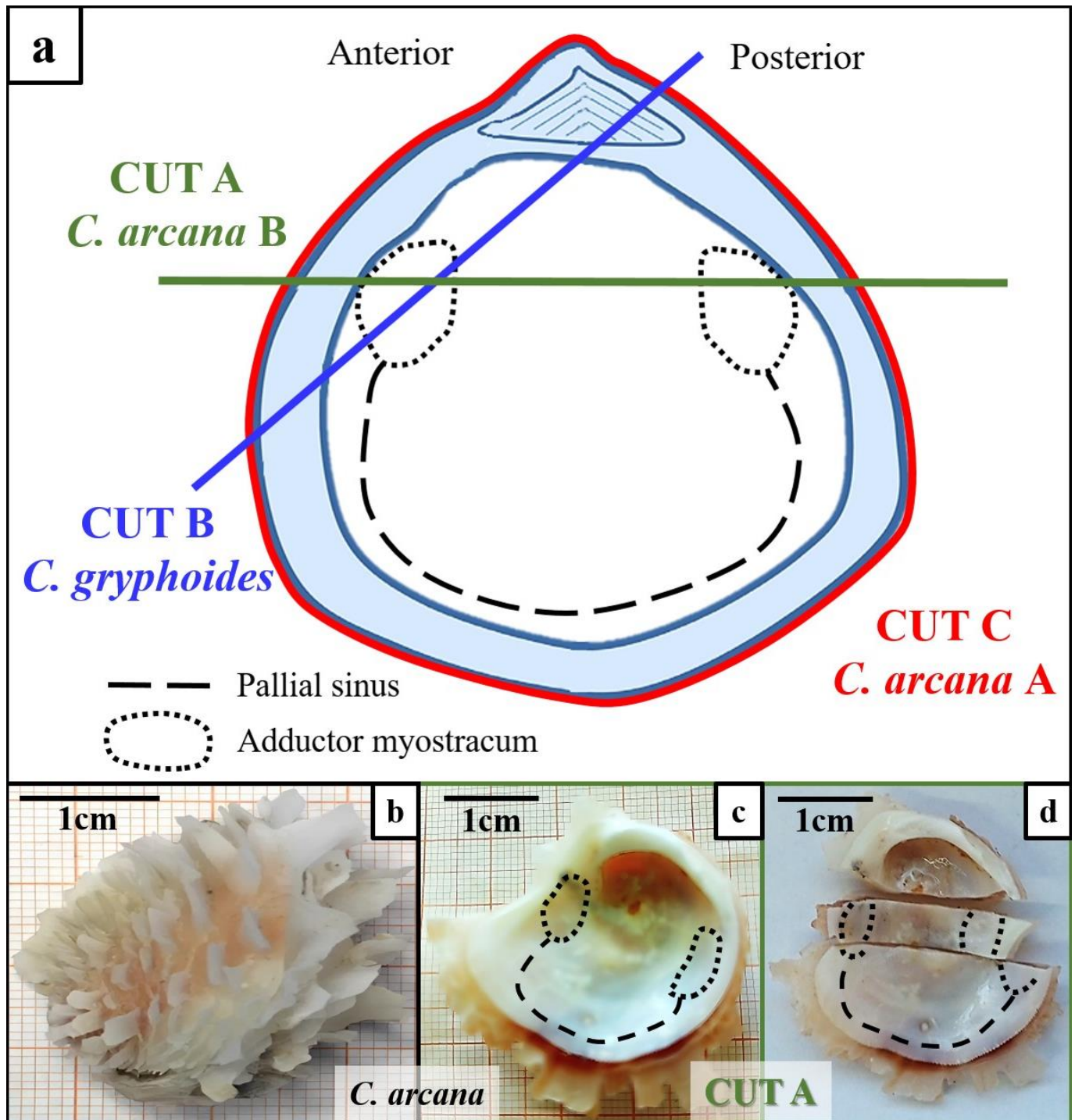


Figure S1. Schematic overview image indicating the direction and position of the different shell cuts performed on the specimens presented in this article (a, modified from Crippa et al. [7]). The valves were cut either crossways, exposing the cross-section of the adductor myostraca (*C. arcana*, cut 1), transversely through both adductor myostraca (*C. arcana*, cut 2) or obliquely through only one adductor myostracum (*C. gryphoides*, cut 3). Valves were cut to expose the adductor myostraca indicated by a dotted line (a, c, d). The ornamentation details (b) and structural morphology of *Chama* shells (c) is indicated by overview images showing the entire shell. The sectioning along cut A is indicated for a *C. arcana* shell (c, d).

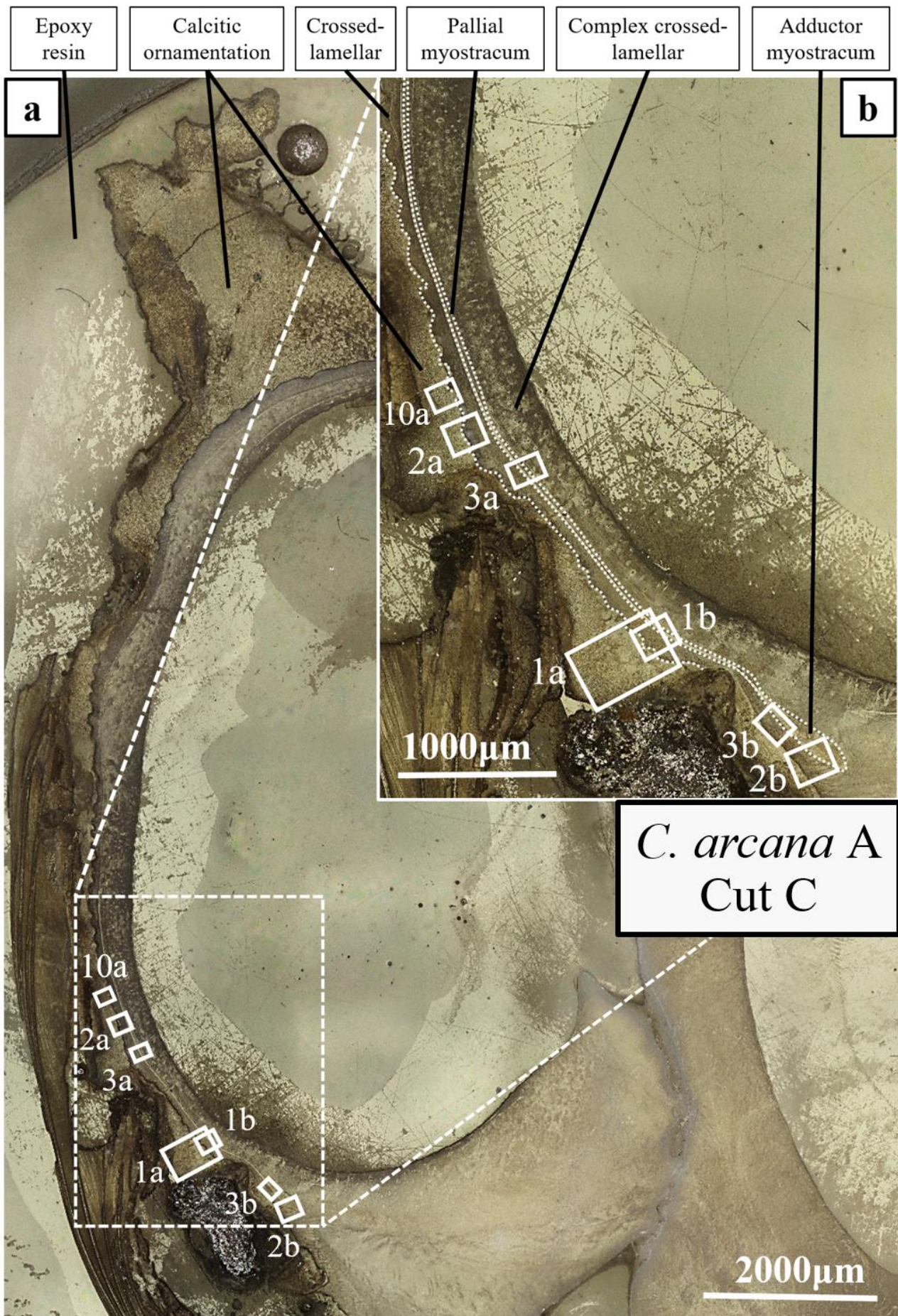


Figure S2. Laser confocal microscopy image depicting the measurement positions for the EBSD scans performed on a *C. arcana* sample that was sectioned crossways (cut 1). The sectioned sample comprises an intricate structure (a) so the measurements were performed in the region near the adductor myostracum. Interfaces of the shell layers are highlighted with dashed white lines in the close-up image (b).

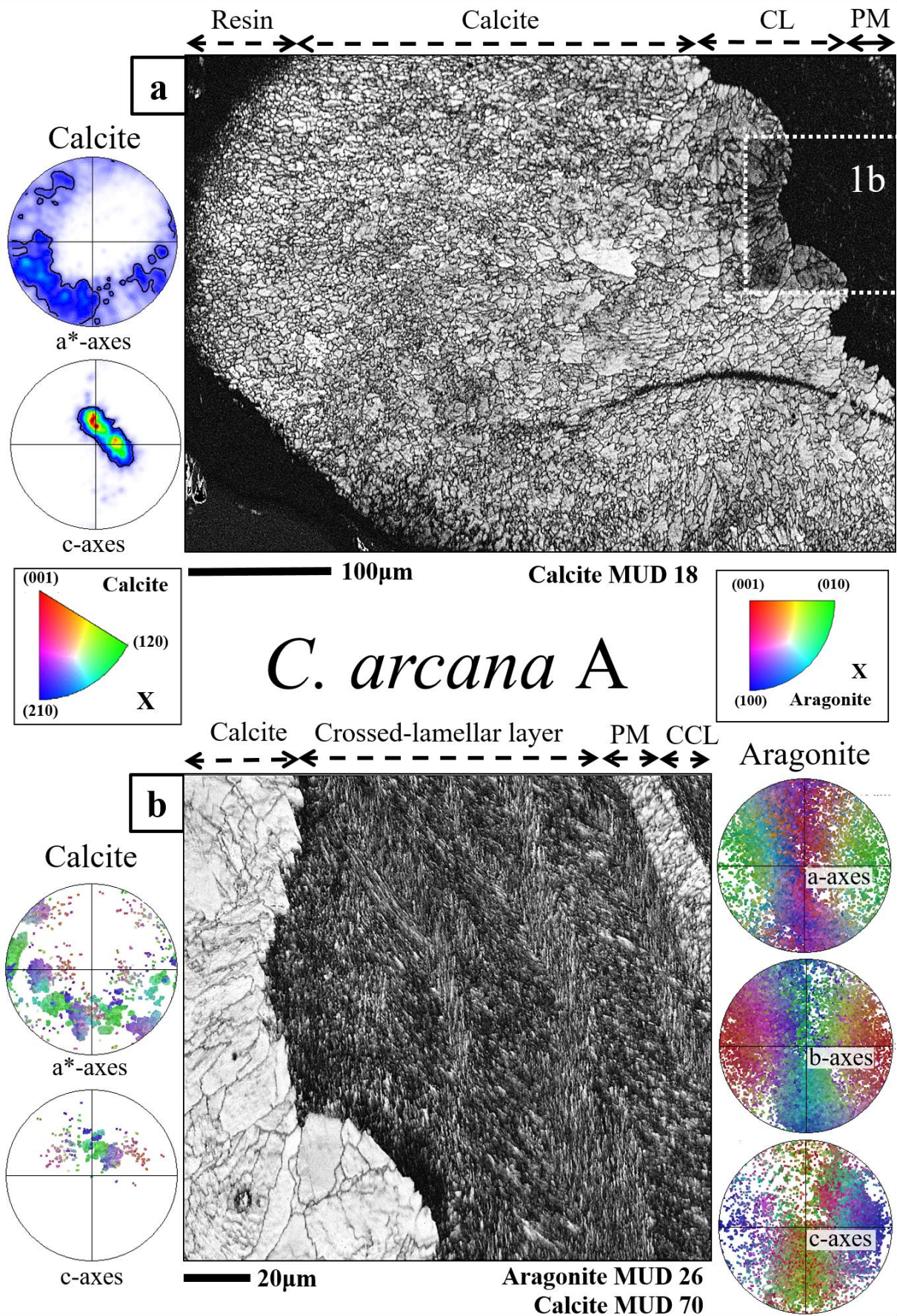


Figure S3. EBSD band contrast images demonstrating the different internal structures present in the applied cut 1 of a *C. arcana* shell. The calcitic ornamentations along the outer shell surface consist of multiple large crystal clusters interlocked into each other (a). The aragonitic crossed-lamellar (CL) layer characteristically comprises multiple sets of differently oriented lamellae, each consisting of small, fibrous crystals (b). The pallial myostracum (MYO) separates the crossed-lamellar layer from the complex crossed-lamellar layer (CCL) on the very inside of the shell (b). The pole figures indicate the individual crystal orientations of the calcitic and aragonitic shell layers (a, b).

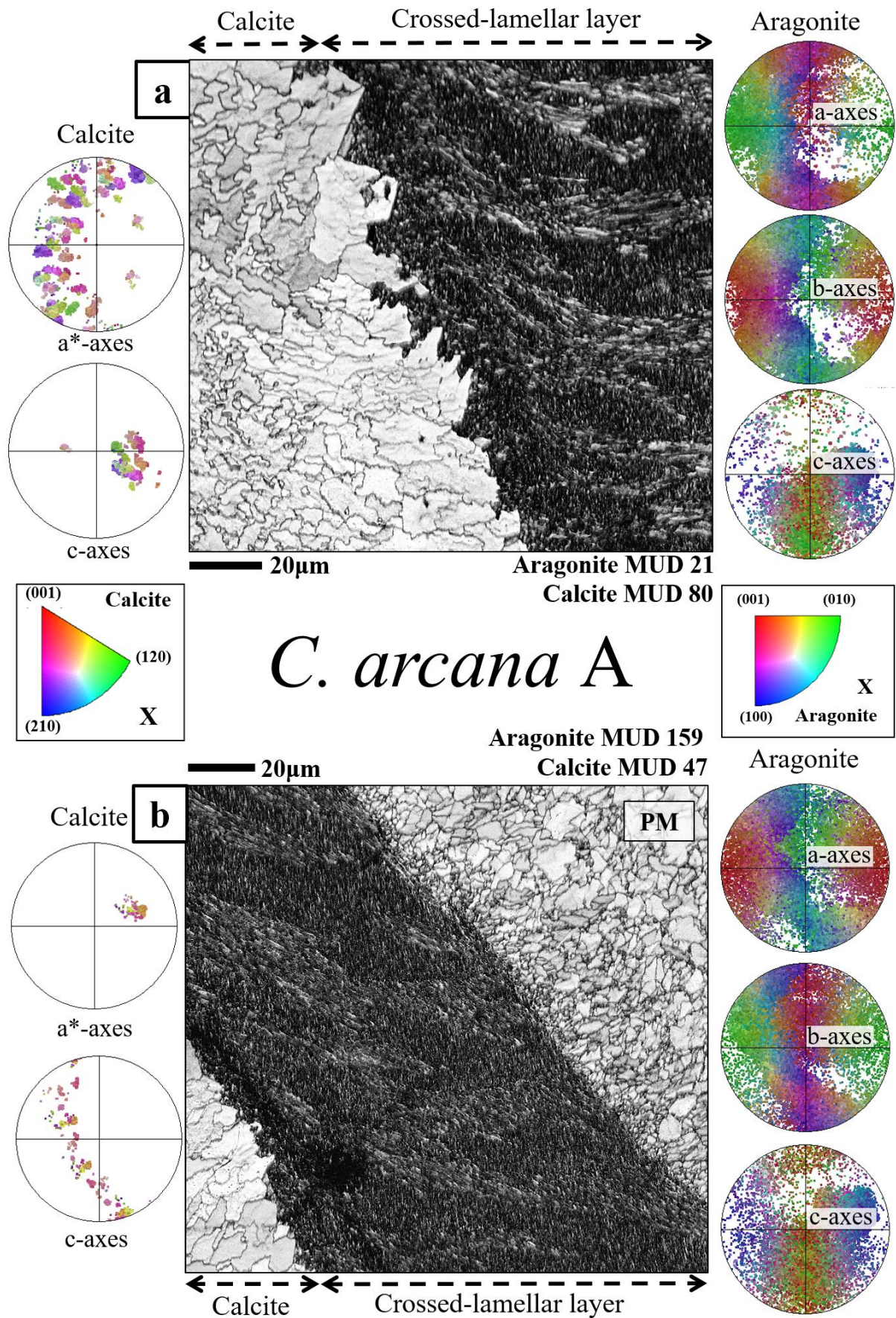


Figure S4. EBSD band contrast images illustrating the interface between the calcitic layer and the aragonitic crossed-lamellar layer observed for the applied cut 1 of a *C. arcana* shell. The crystals within the calcitic layer show a complex and fractal-like interpenetration. Towards the inner shell surface, the crossed-lamellar layer transitions into the adductor myostracum (AM, b). The pole figures display the individual data points of the crystal orientations in the calcitic and aragonitic layers. The texture of both layers is axial, however, the calcitic layer is rather co-oriented and aragonitic crystal orientations vary significantly.

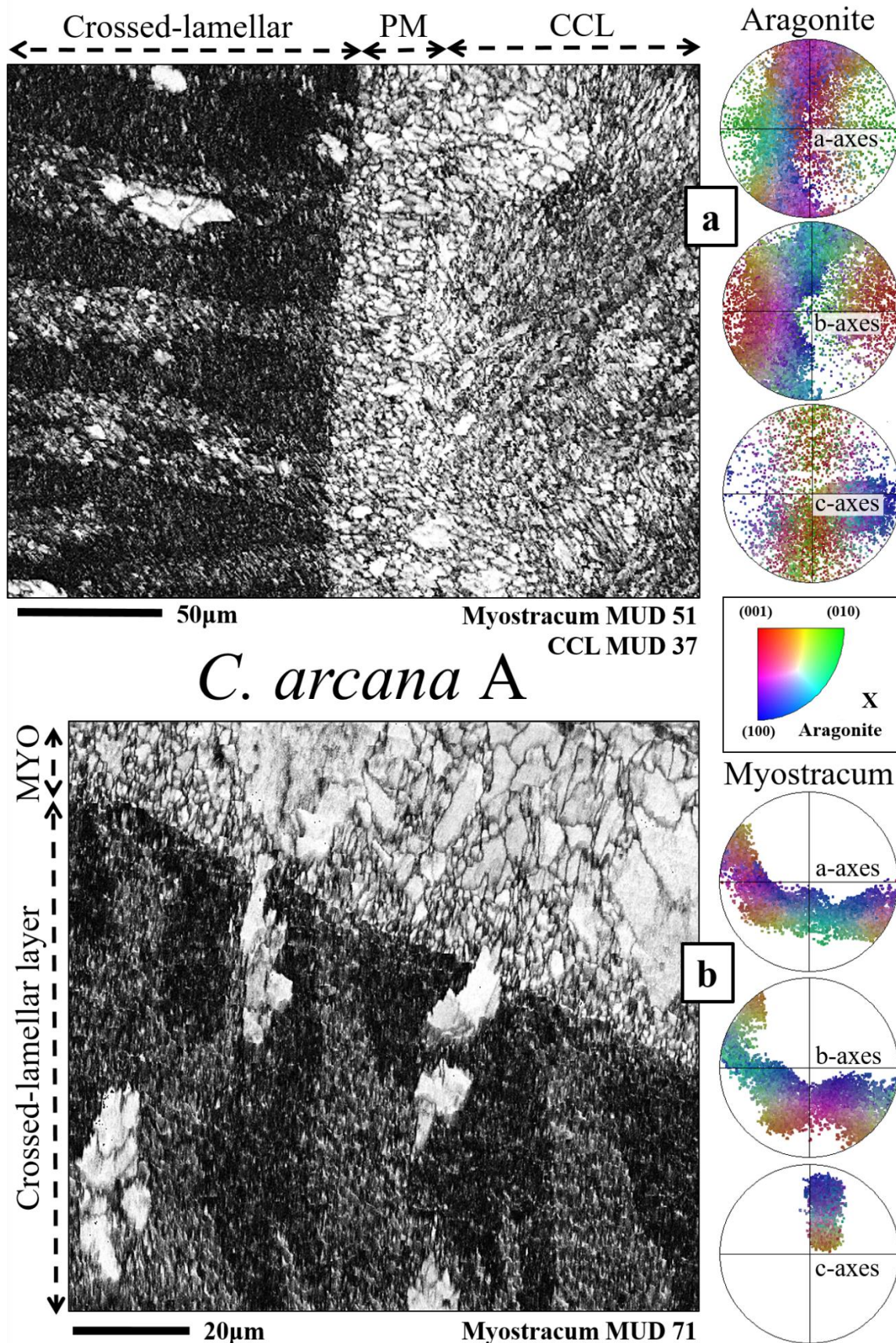


Figure S5. EBSD band contrast images depicting the interfaces within the different aragonitic layers of a *C. arcana* shell sectioned crossways (cut 1). The interface between the pallial myostracum and the complex crossed-lamellar layer (CCL) is indistinct and vague (a). The crossed-lamellar layer, however, shows a straight and rather sharp interface with the pallial (PM, a) and adductor myostraca (AM, b). A peculiarity highlighted in the two scans is the occasional presence of crystal assemblies consisting of large (around 10 μ m) grains appearing in the interface region of the crossed-lamellar layer (yellow stars in a, b), their morphology resembling myostracum crystals with high crystal co-orientation and intensity of the Kikuchi bands. The pole figures indicate the individual crystal orientations of the pallial and the adductor myostracum in the two respective scans (a, b).

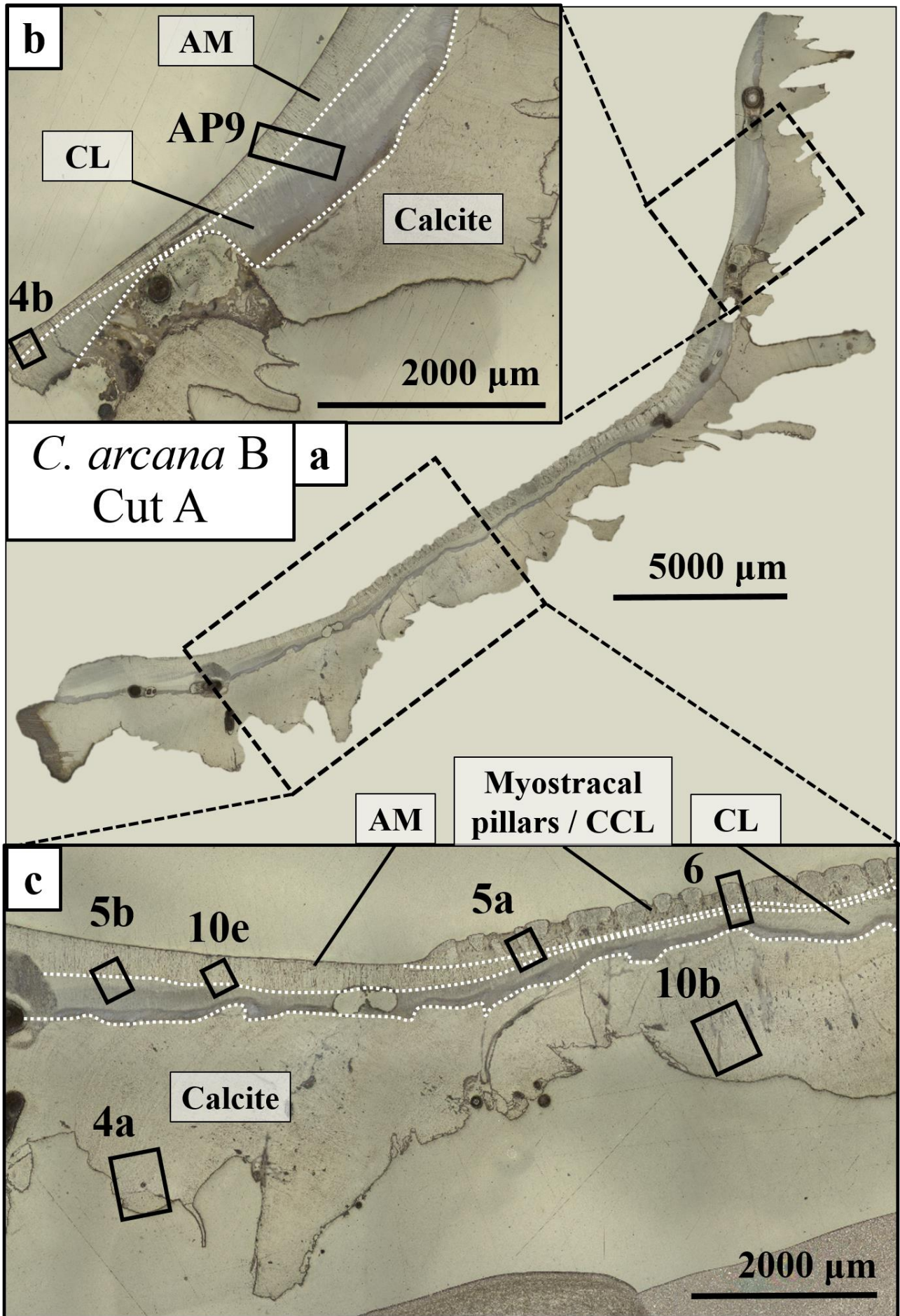


Figure S6. Laser confocal microscopy images depicting the measurement positions for the EBSD scans performed on a transversely cut *C. arcana* shell (cut 2). Two measurements were performed on the posterior (b) and six measurements on the anterior end (c). The interfaces of the respective layers are highlighted with dashed white lines (b, c). AM: Adductor myostracum, CL: Crossed-lamellar layer, CCL: Complex crossed-lamellar layer.

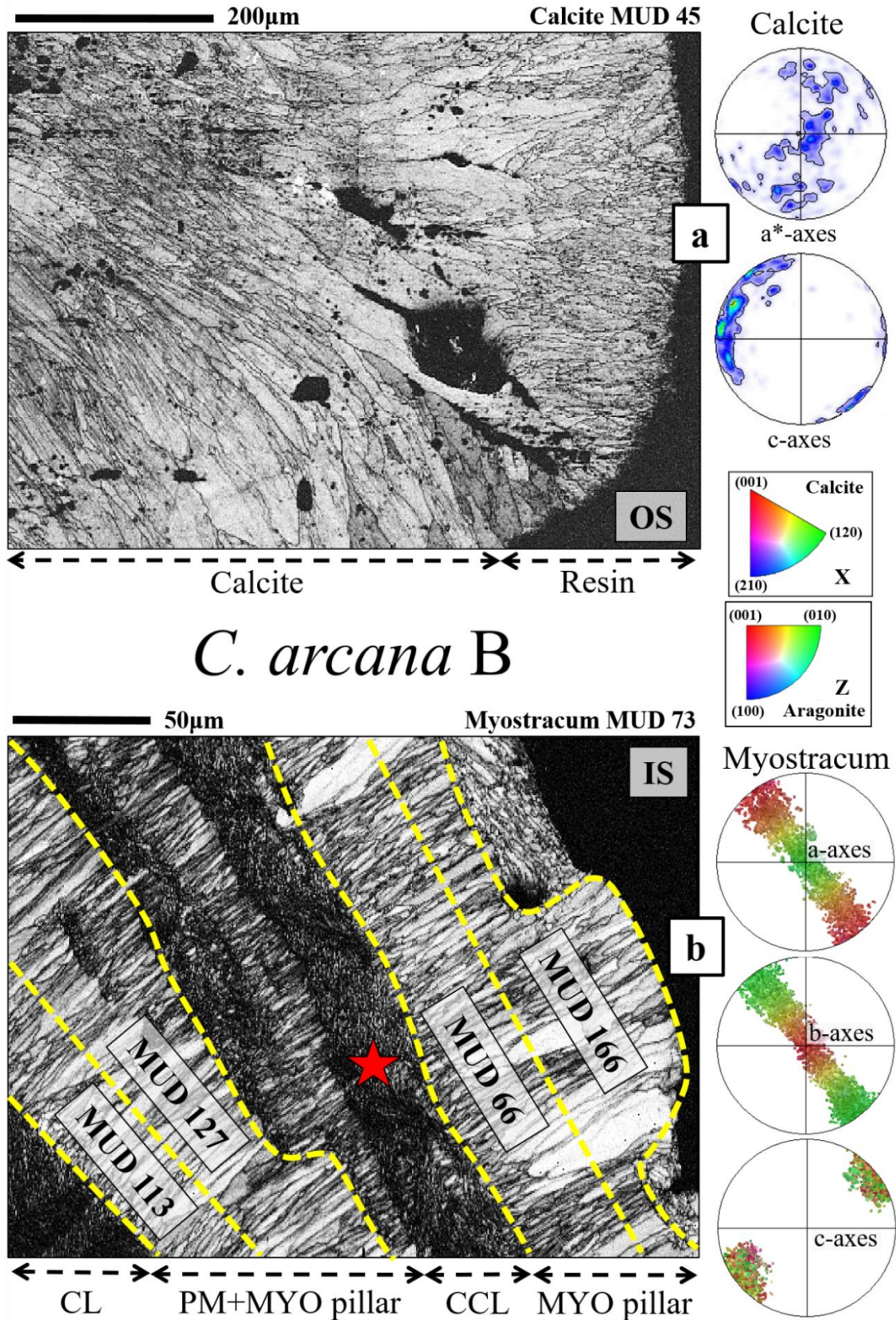


Figure S7. EBSD band contrast images depicting the different microstructures observed for the applied transverse cut 2 of a *C. arcana* shell. The calcitic shell ornamentalations along the outer shell surface (OS) comprise crystal units that follow an intricate interlocking mechanism (a). In the aragonitic section of the shell, the pallial myostracum (MYO) comprises small, isotropic crystals close to the interface with the crossed-lamellar layer (CL, b). The pallial myostracum exhibits a competitive growth mechanism that causes the overall crystal size and co-orientation strength (indicated by MUD values of subsets indicated by dotted yellow lines) to increase rapidly towards the inner shell surface (IS). When interrupted by a continuous sheet of complex crossed-lamellar (CCL) layer (red star in (b)), the competitive growth mechanism of the myostracal pillar restarts. The pole figures for the calcitic and myostracum areas of the two scans show an axial texture (a, b).

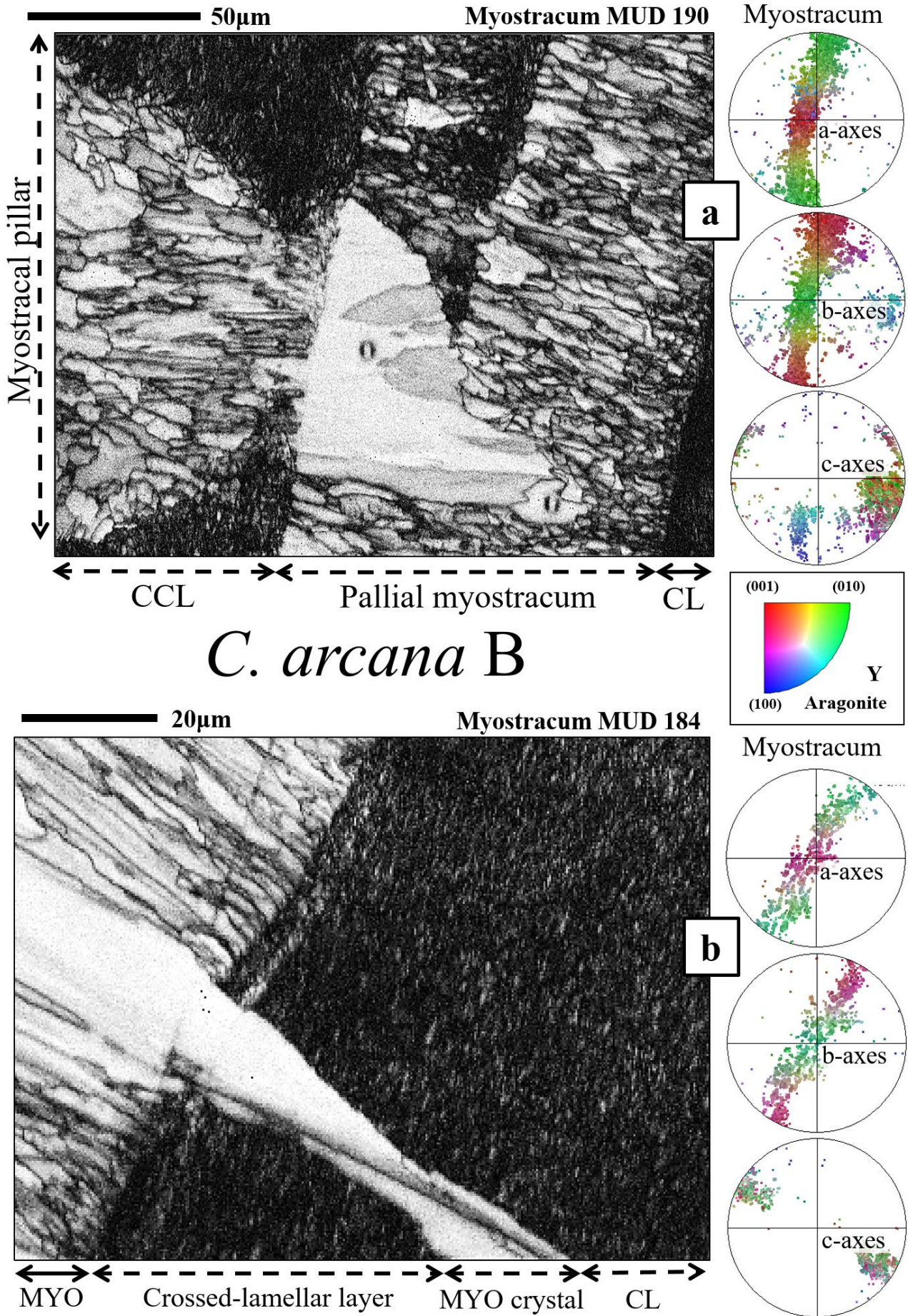


Figure S8. EBSD band contrast images depicting large, anomalous myostracum (MYO) crystals observed for the applied transverse cut 2 of a *C. arcana* shell. The highlighted sizeable crystals can occasionally be found in the pallial (red star in a) and the adductor myostracum (AM, yellow star in b) and show a peculiar microstructure. The pole figures display the individual data points of the crystal orientations for the myostracum layers that show an axial texture.

C. arcana B

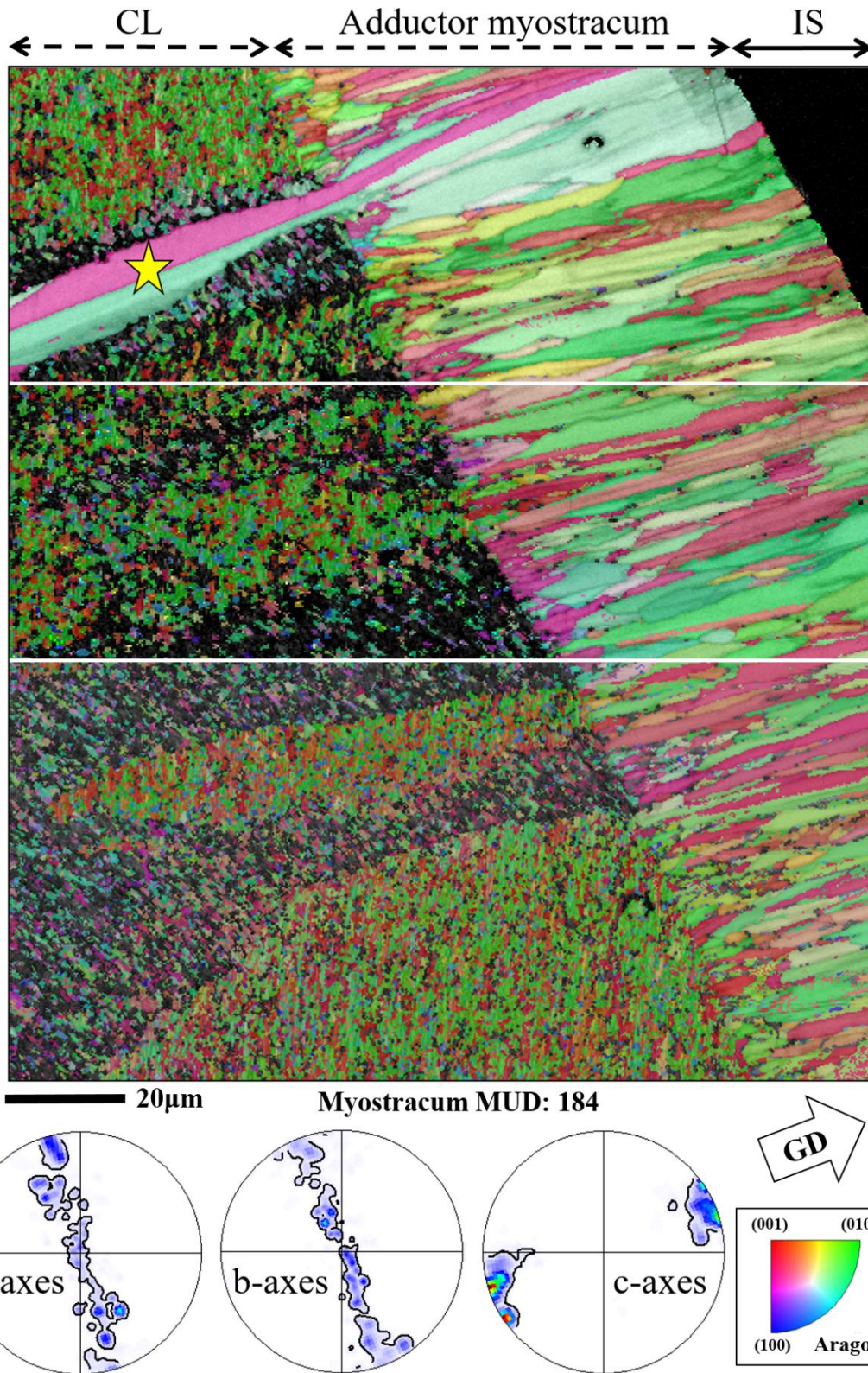


Figure S9. EBSD scans depicting the interface between the crossed-lamellar layer (CL) and the myostracum for the applied transverse cut 2 of a *C. arcana* shell. The EBSD map is composed of three individual scans with overlapping positions. The white lines indicate the borders of the respective measurements. The composite map highlights the transition of the crossed-lamellar sets into the myostracum. Along this interface, the orientations of the rearmost crossed-lamellar crystals and the adjacent myostracum crystals correlate. Due to the competitive growth mechanism, the pattern is quickly lost towards the inner shell surface (IS) as the crystals increase in size and prismatic shape. Similar to Fig. 8b, a substantial crystal (indicated by a yellow star) traverses both shell layers. The pole figures show the orientational probability density distribution for the myostracum area of the composed scan and depict an axial texture. The growth direction (GD) is indicated with a white arrow.

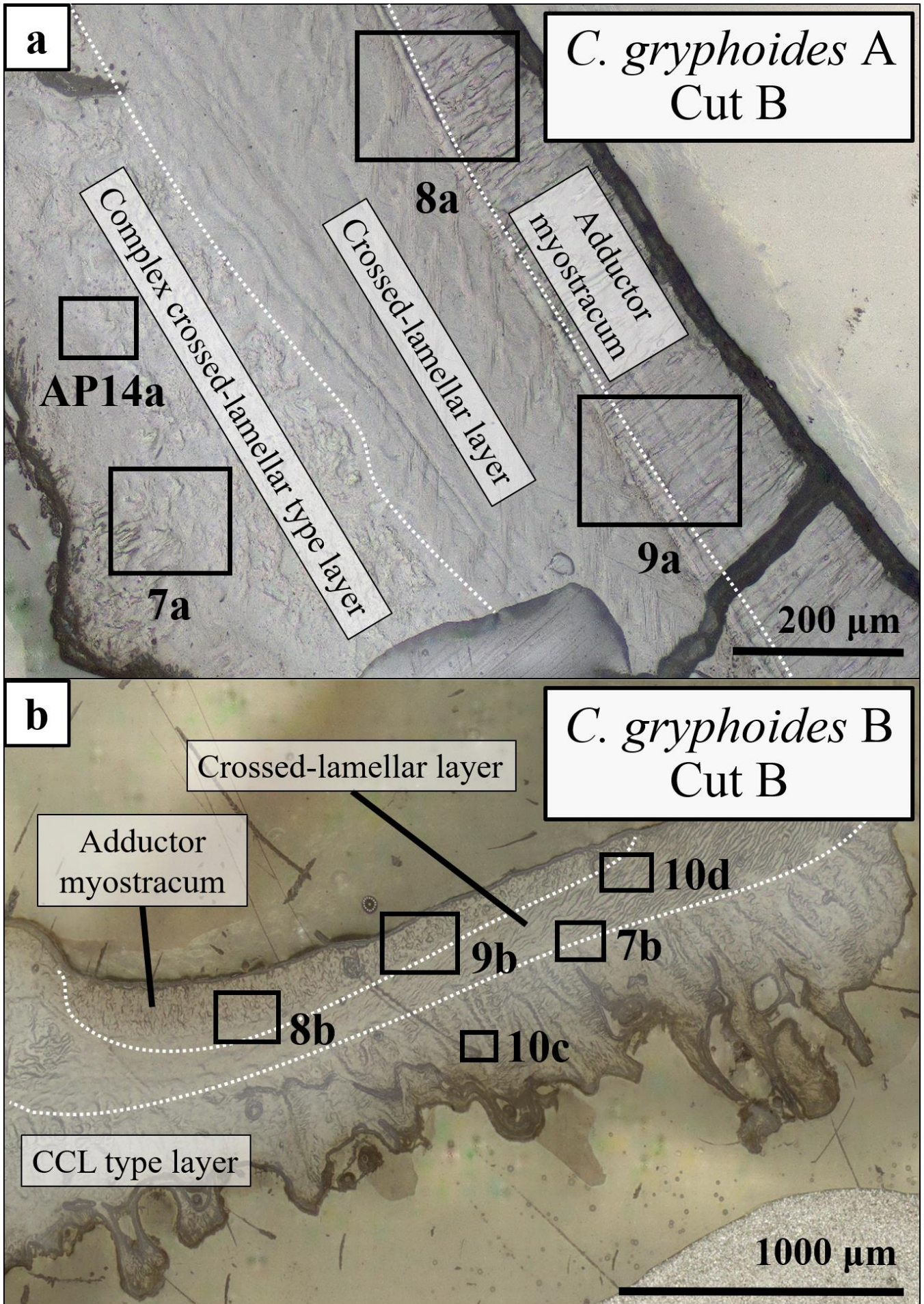


Figure S10. Laser confocal microscopy images depicting the measurement positions for all *C. gryphoides* EBSD scans. A total of nine measurements were performed on the two samples sectioned obliquely (cut 3). The interfaces of the respective layers are highlighted with dashed white lines (a, b). CCL: Complex crossed-lamellar.

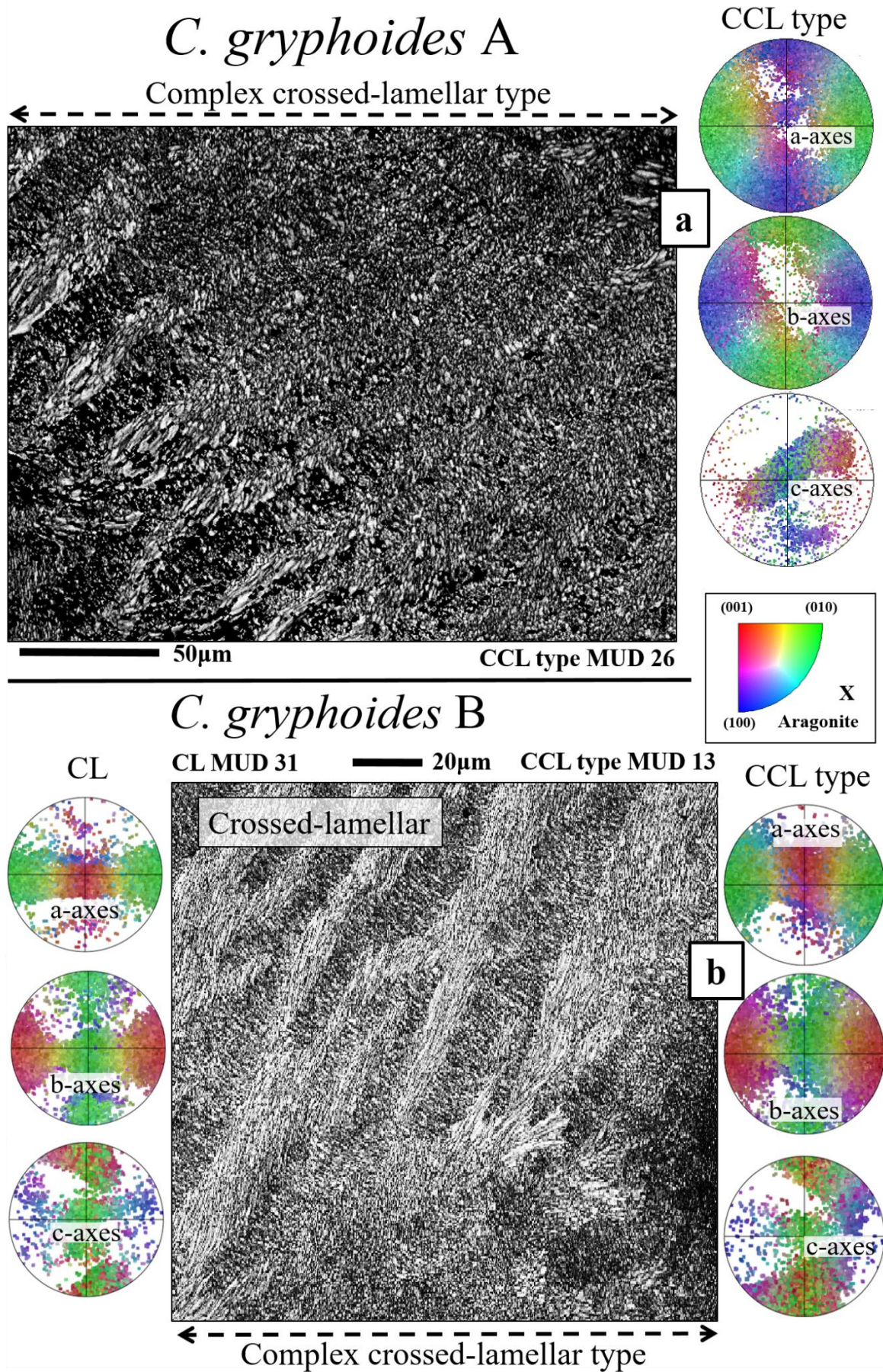


Figure S11. EBSD band contrast images displaying the microstructure of the complex crossed-lamellar (CCL) type layer for different shells of *C. gryphoides* sectioned obliquely (cut 3). The complex crossed-lamellar layer comprises first-order-lamellar blocks arranged in a complex pattern (a) and has a rather smooth changeover into the complex crossed-lamellar layer (b). The texture is shown by the pole figures indicating individual data points of the crystal orientations for the respective layers.

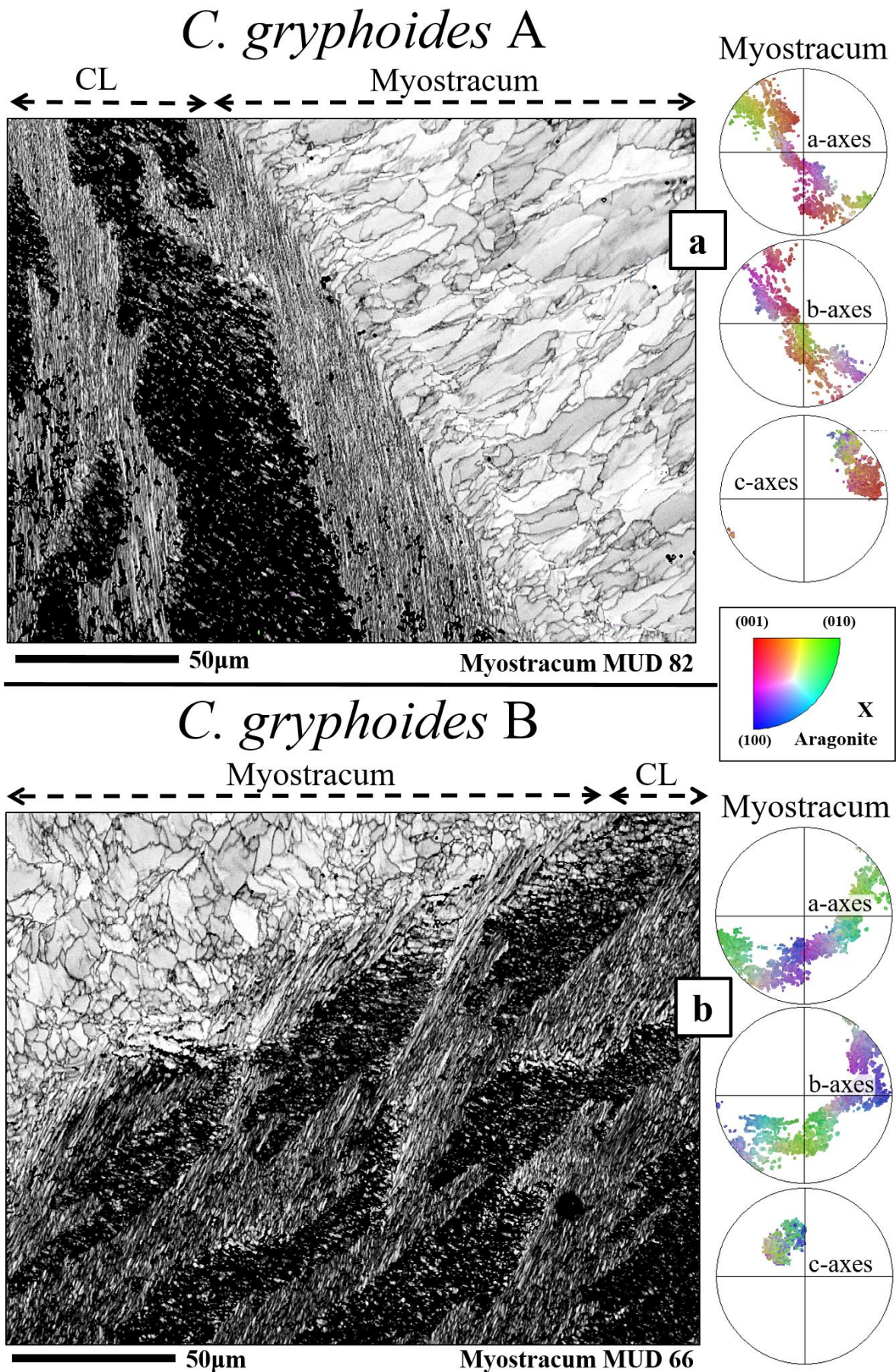


Figure S12. EBSD band contrast images depicting the interfaces between the crossed-lamellar layer (CL) and the adductor myostracum observed for the two obliquely sectioned (cut 3) *C. gryphoides* shells. The crystals within the crossed-lamellar layer are small and prismatic, while the competitively grown myostracum crystals get increasingly large towards the inner shell surface (a, b). The pole figures display the individual data points of the crystal orientations for the myostracum sections that show an axial texture. The double maxima for the c-axis orientations are a relic of the crossed-lamellar crystal orientation pattern and the a- and b-axis orientations scatter significantly (a, b).

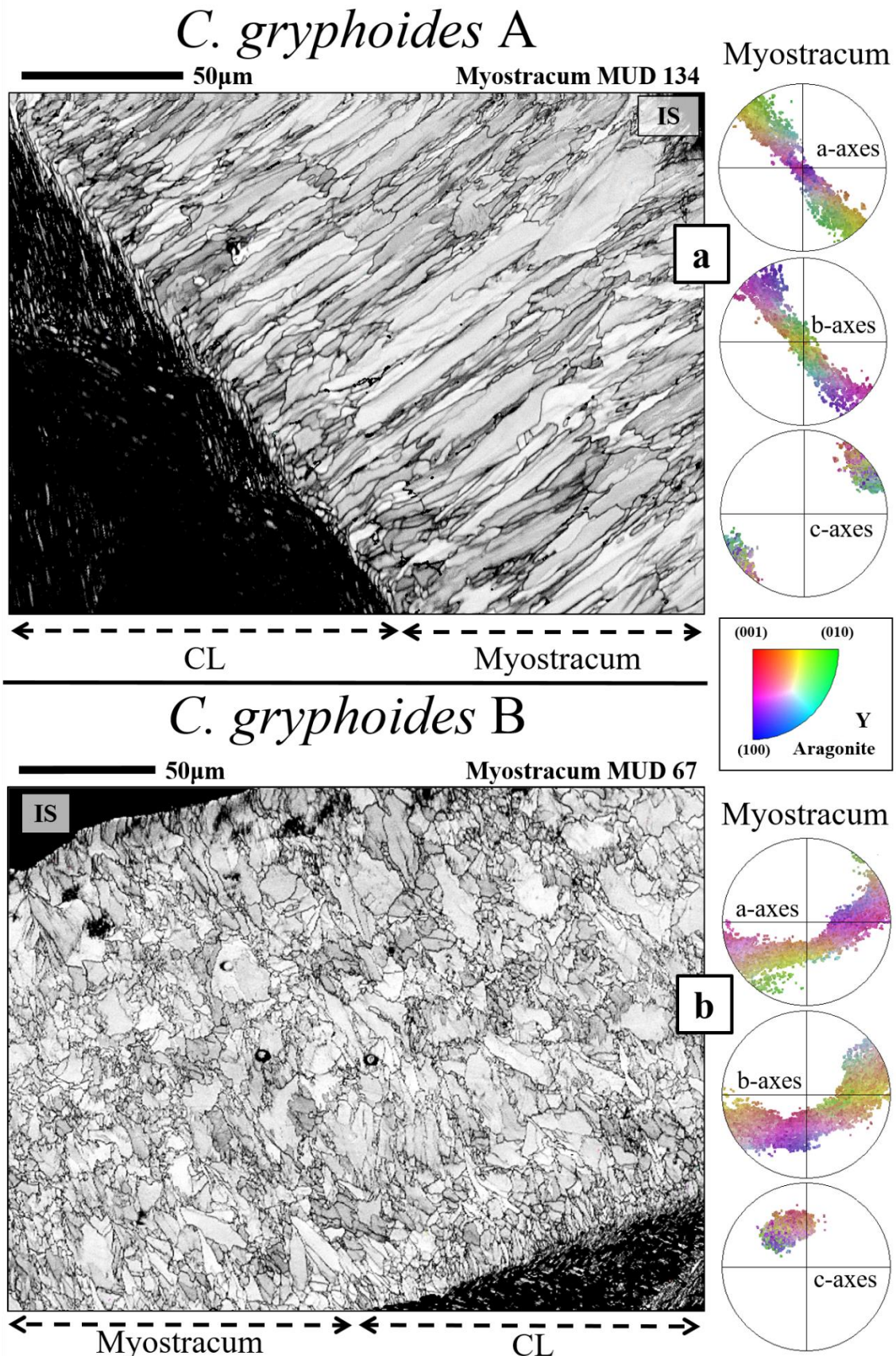


Figure S13. EBSD band contrast images depicting the microstructures of adductor myostraca observed for the two applied cuts (cut 3) of *C. gryphoides* shells. Due to slightly deviating cutting directions between the two shells, the exposed microstructures depict different crystal morphologies. The crystals of the first shell are prismatic, the EBSD map exemplifies that their grain boundaries appear irregular and disorganized (a). In the second shell, the scan illustrates the irregular grain morphologies of the myostracum crystals (b). The illustrated microstructure of the myostracum in both scans (a, b) results from the competitive growth prevailing towards the inner shell surface (IS). The pole figures display the individual data points of the crystal orientations for both myostracum layers that show an axial texture.

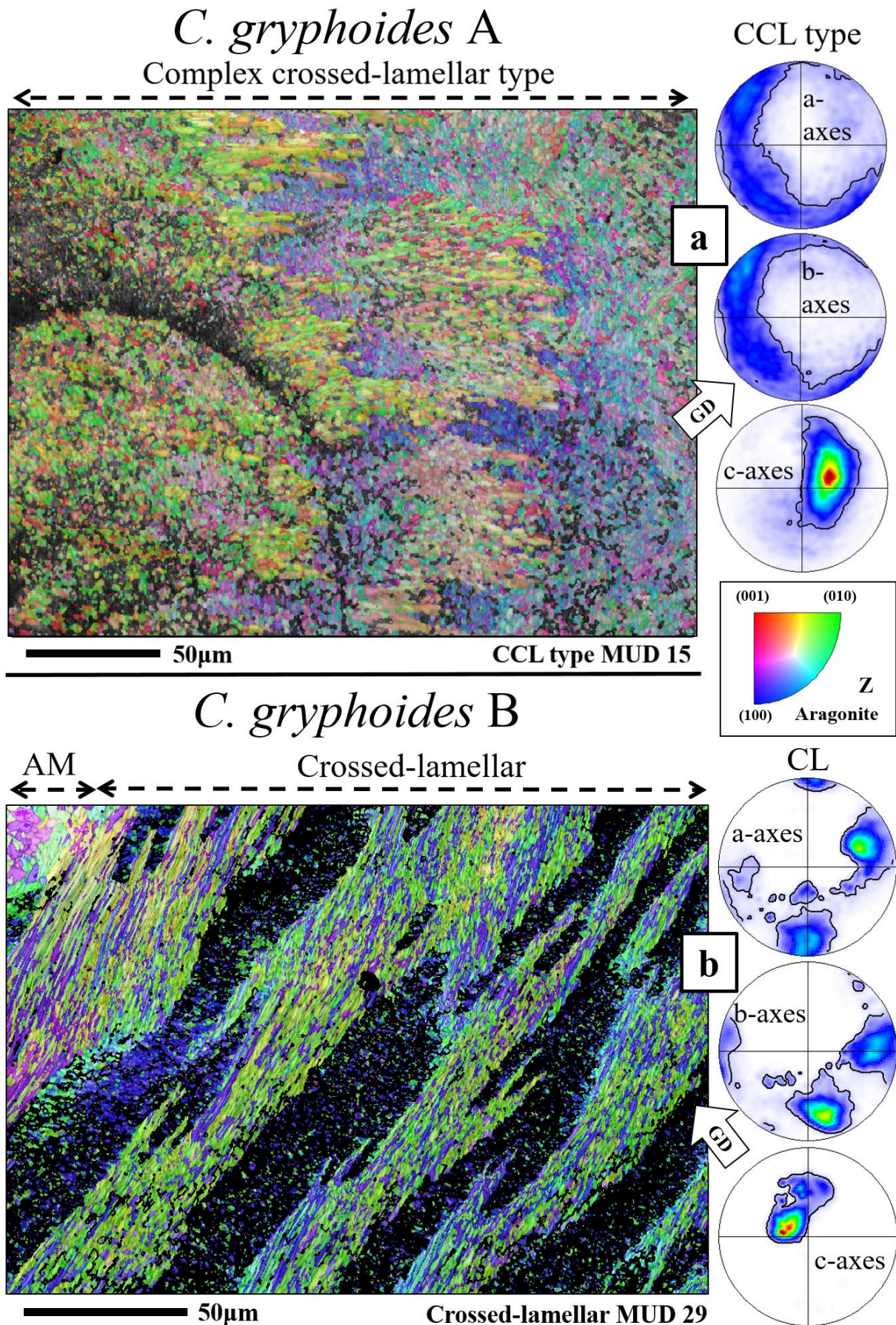


Figure S14. EBSD band contrast images depicting changeovers observed for the two applied cuts of *C. gryphoides* shells. The first scan depicts the microstructure of the complex crossed-lamellar (CCL) type layer (a). In the second shell, the scan illustrates the microstructure of the crossed-lamellar shell and its changeover into the adductor myostracum (b). The pole figures display the orientational probability density distribution in the CCL type and the crossed-lamellar layers. The CCL type layer has an axial texture (a), and the complex crossed-lamellar layer shows a 3D “single-crystal-like” texture. The growth direction (GD) of each scan is indicated with a white arrow.